Bound-state resonances and interaction potential of helium scattered by graphite (0001)

G. Boato, P. Cantini, C. Guidi, and R. Tatarek
Gruppo Nazionale di struttura della Materia del Consiglio Nazionale delle Ricerche, Istituto di Scienze Fisiche dell'Universitá, Genova, Italy

G. P. Felcher
Argonne National Laboratory, Argonne, Illinois 60439
(Received 7 May 1979)

The present study was undertaken on the basis of two motivations. On one hand, the He-graphite system is ideally suited for the study of bound-state resonances and of band-structure effects in atom-surface scattering; on the other, an accurate determination of the interaction of a He atom with the basal plane of graphite is of great value for the study of physical adsorption and the properties of two-dimensional adsorbed layers. Elastic diffraction measurements of quasimonochromatic He atoms from a low-temperature graphite (0001) surface are reported here. From the angular position of bound-state resonance minima in the specular intensity, the laterally averaged potential V_0 is found to give rise to five discrete levels with energies of 11.98, 6.33, 2.85, 0.99, and 0.17 meV. Band-structure effects taking place at the crossing of resonances were studied for a variety of experimental conditions. From the observed splitting, it is confirmed that only the first Fourier component V_{10} is making a relevant contribution to the periodic part of the potential and the matrix elements $\langle\chi_m|V_{10}|\chi_n\rangle$ are evaluated. The energy levels and the matrix elements are used to derive information on the gas-surface potential. V_0 is found to be well represented by a Lennard-Jones 5-10 potential, with a well of 15.70 meV. V_{10} is also represented by a model potential, and the overall implication of the results is discussed in the light of other experimental and theoretical findings. A brief description of the line shapes of the resonances and an evaluation of the linewidths are also given; these are compared with recent theoretical studies.

I. INTRODUCTION

The importance and value of a careful study of the interaction potential between a neutral atom and the basal plane of graphite have been well emphasized in the literature.[1] The thermal-atom diffraction technique is especially suited to such a study, particularly if a low-energy beam is used to enhance the contribution of resonance scattering[2]; using this technique, valuable information may be gathered on the attractive part of the potential, particularly through the use of band-structure effects.[3]

Two preliminary papers on this subject were published by Boato *et al.*[4,5] In the first one, carried out with a beam of helium atoms at room temperature, the feasibility of the experiment was proven. The sharp diffraction pattern gave information on the corrugation of the surface; using the hard-wall model with a well, a maximum-to-minimum corrugation of 0.21 Å was found, about one-third of that present in LiF(001). Only the first Fourier component of the surface corrugation was found to be appreciable. From the bound-state resonances four levels ϵ_m of the laterally averaged potential were determined; this allowed a first comparison with adsorption data.[6,7] In the second paper, a more careful study of the bound-state resonances was carried out, using a He beam produced by a liquid-N_2-temperature source. More accurate values for the levels were given and band-structure effects were evidenced by studying selected cases of split resonances. The significant contribution of the first Fourier component alone to the periodic part of the potential was confirmed by the observed splittings. The present study is a complete analysis of the resonance structures observed with a low-temperature beam. The absolute values of the resonances were reevaluated and compared with those obtained by Derry *et al.*[8] A thorough study of resonance crossings was carried out: line shapes of isolated and interacting resonances were accurately determined and, above all, band-structure matrix elements were derived from energy splittings for all combinations of vibrational levels.

We review the main points of the diffraction process: atoms with incident wave vector $\vec{k}_i$ $(\vec{K}, k_z)$ are scattered by a perfect surface in diffraction channels corresponding to the reciprocal-lattice vectors $\vec{G}$ of the surface. A bound-state resonance (BSR) occurs whenever the incident beam of particles of mass m satisfies the condition

$$k_i^2 = (\vec{K}+\vec{G})^2 + 2m\epsilon_m/\hbar^2 , \tag{1}$$

where $\vec{G}$ corresponds to a *closed* diffraction channel and the ϵ_m's are the discrete levels of the zero Fourier component of the gas-surface potential $V(\vec{R}, z) = \sum_{\vec{G}} V_{\vec{G}} \exp(i\vec{G}\cdot\vec{R})$. In this free-atom approximation the loci of the resonances are circles

in the reciprocal plane. The further components of the potential (of which V_{10} is usually the largest, and the only one detectable in graphite) are rather negligible in comparison with V_{00} everywhere in the $\vec{K}$ plane except close to the crossings of two resonances. Here the simple perturbation formula applies:

$$[E_i - \hbar^2(\vec{K}+\vec{G}_1)^2/2m - \epsilon_m][E_i - \hbar^2(\vec{K}+\vec{G}_2)/2m - \epsilon_n] = |V^{mn}_{\vec{G}_1-\vec{G}_2}|^2 , \quad (2)$$

where the relevant matrix elements are given by

$$V^{mn}_{10} = \int \chi_m(z) V_{10}(z) \chi_n(z)\, dz , \quad (3)$$

χ_m and χ_n being eigenfunctions of the laterally averaged potential $V_0(z)$. The energy splittings are simply $|2V^{mn}_{10}|$. The relations given here namely fix the kinematic conditions under which BSR's occur. The resonances give rise to a disturbance in the experimentally observable intensities of the diffracted beams, which may have the form of a minimum, a maximum, or a more complex appearance. For the case at hand—the diffraction of helium from the hexagonal (0001) plane of graphite—a self-consistent body of observations was collected and sufficient theoretical understanding reached to allow an unambiguous assignment of resonance energies from the experimental spectra. The experimental matrix elements are presented in Table II and their relation to model gas-surface potentials is discussed. A more detailed description of the experimental shape of the resonance lines is also given. It is our hope that the data presented here will be of assistance in reaching a better understanding of atom-surface scattering and will stimulate the formulation of more accurate gas-surface potentials.

II. EXPERIMENTAL PROCEDURE

The experimental setup, basically the same as that used in previous scattering experiments, has been described elsewhere.[9] It will suffice to outline here only some of the details that are important in BSR experiments.

The present data refer to the scattering of a He beam produced with a supersonic nozzle source at low temperature ($T_0 = 103$ K); the beam is nearly monoenergetic ($\Delta k_i/k_i \sim 2\%$), with wave vector $k_i = 6.49$ Å^{-1} (corresponding to an energy $E_i = 22$ meV). In order to determine the inherent width of a BSR, the beam is also well collimated ($\Delta\theta \sim 0.15°$) and narrow (~0.4 mm at the crystal).

Natural graphite specimens were used throughout. Each crystal was cleaved in air, fastened with Aquadag to the sample holder, and then heated in an ultrahigh vacuum for several hours at 700 K. Occasionally the specimens showed some misorientation among adjacent twinned crystals. The present data were obtained with four different specimens, normally chips with a lateral size of 5–6 mm and a thickness of 0.2 mm. During the measurements, the specimens were maintained at a temperature $T_s \sim 80$ K.

The crystal holder could be rotated independently around three perpendicular axes so that the out-of-plane angle, the polar angle, and the azimuthal angle could be changed. The first movement was used only to orient the crystal perpendicularly to the plane of the detector. The other movements were used to change the angle of incidence of the beam.

BSR structures in the specular beam were determined by measuring its intensity as a function of the incident angle θ for a set of azimuthal angles ϕ. The angle ϕ was varied over a range of 30°, thus covering all the directions of the hexagonal (0001) plane of graphite; its origin was chosen along the ⟨10⟩ direction. The changes in ϕ were obtained by rotating an external driver. Since 3,450 turns of the driver are necessary to change ϕ by 360°, each turn corresponds to $\Delta\phi \sim 0.1°$, which can be roughly considered to be the azimuthal resolution. At each ϕ the scanning was performed by changing the incident polar angle by as little as one-sixth of a degree (and in some exceptional cases by only one-twelfth). Almost all the interesting regions for strong resonances were explored. BSR crossings were observed under different conditions, thus allowing for a detailed study of this interesting phenomenon.

In spite of the very good angular resolution there was some ambiguity in fixing the zeros of the angles of incidence (θ, ϕ). In order to determine with accuracy the two principal azimuths, $\phi = 0°$ and $\phi = 30°$, one of the following procedures was adopted. (a) At small θ's, where few weak BSR's are present, the in-plane intensity of a first-order peak, e.g., (10) and (11), respectively, was maximized; this method brought about an error of ~1°. (b) At intermediate θ's, from 30° to 60°, the specular intensity was plotted vs ϕ and the principal azimuth was determined by the symmetry of the minima, which characterize bound-state resonances: with this method uncertainty was reduced to ~0.3°. (c) Even better precision was obtained near grazing incidence. Here again two strong BSR's associated with $\vec{G}$ vectors that are symmetrically placed with respect to the incoming beam cross each other in each principal azimuth; the resulting minimum was twice as deep as the two isolated minima. The angular location of the deepest minimum gave for both directions the

TABLE I. Elastic diffraction probabilities ($\times 10^2$) for He-graphite(0001). $\theta_i = 5°$.

Incident wave vector	Miller indices (20)	(11)	(10)	(00)	($\bar{1}$0)	($\bar{1}\bar{1}$)	($\bar{2}$0)
$k_i = 6.49$ Å^{-1}	···	0.33	2.60	18.1	3.27	0.44	···
$k_i = 11.05$ Å^{-1}	0.29	0.77	2.33	3.23	2.31	0.82	0.42

azimuth with a precision better than 0.1°.

It was much more difficult to determine with adequate precision the zero in the polar angle θ. The method previously used, that of aligning the beam parallel to the plane of the crystal holder, was not effective in the case of graphite, since the specimen surface was not necessarily parallel to this plane and since the beam was usually moved laterally to reach a more perfect area of the crystal. In order to fix the zero of θ, the alternative method of measuring (near normal incidence) the angle between the incoming and the specular (00) beam and dividing it by 2 was adopted. This procedure is not completely free from misalignment errors, for it is assumed that the illuminated region of the crystal is exactly at the center of the detector goniometer. However, the eventual errors introduced thereby affect only the absolute values of ϵ_m (see Sec. III) and not the determination of the energy splittings, which is the major aim of the present work.

III. EXPERIMENTAL RESULTS

A. Corrugation of surface

With the source at $T_0 = 103$ K the diffracted intensity was measured at incidence near normal. The shape of the diffraction peaks is accounted for by almost pure elastic scattering; their position, by the hexagonal lattice of graphite with $a_0 = 2.456$ Å. Diffraction probabilities were derived from the diffraction pattern by the usual procedure.[9] Typical values at $\theta \simeq 5°$ in the two principal azimuths $\phi = 0°$ and $\phi = 30°$ are shown in Table I along with similar values obtained with the source at room temperature. By using the corrugated hard-wall model with a well and the eikonal approximation,[11] these probabilities are well accounted for by a corrugation parameter $\zeta_{10} = 0.023 \pm 0.002$ Å. Only the first Fourier component ζ_{10} of the shape function $\zeta(\vec{R}) = \sum_{\vec{G}} \zeta_{\vec{G}} \exp(i\vec{G}\cdot\vec{R})$ is needed. No dependence of the corrugation on the incident energy is apparent.

B. Observation of resonances

Figures 1 and 2 show scans of the specular intensity along the two principal azimuths, $\phi = 0°$ and $\phi = 30°$, respectively. The center portion of Fig. 1 was published in a previous paper[5]: here deep minima were observed, which we related to the (10) and to the (01)-(1$\bar{1}$) unsplit BSR's. The assignment of the resonance labels proceeded as follows. Suppose that the minima represent

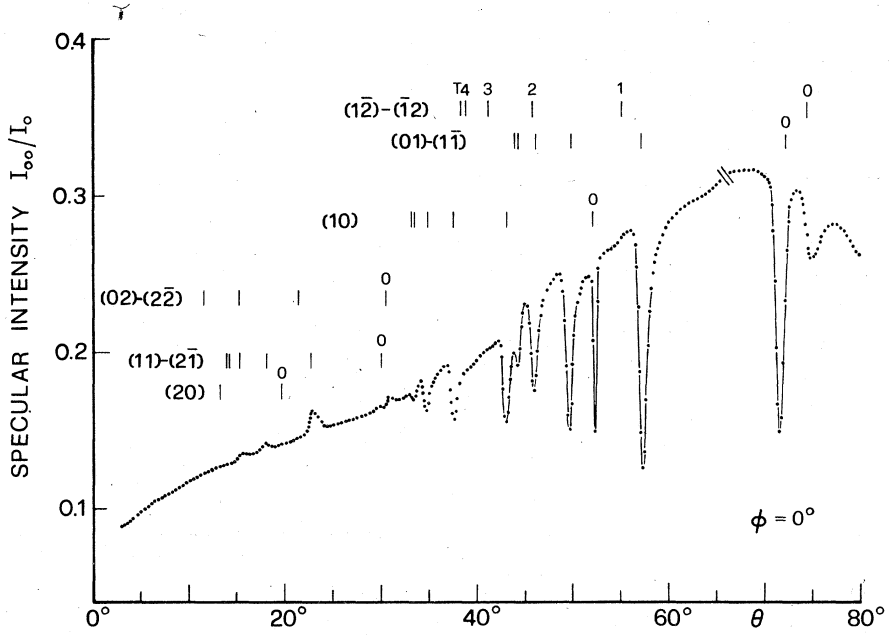

FIG. 1. Specular intensity at $\phi = 0°$ vs incident angle θ. Vertical bars indicate location of BSR's, using Eq. (1) with revised energy levels given in Sec. III. Levels are labeled by reciprocal-lattice vector indices and by level index going from 0 to 4. T shows calculated location of the threshold.

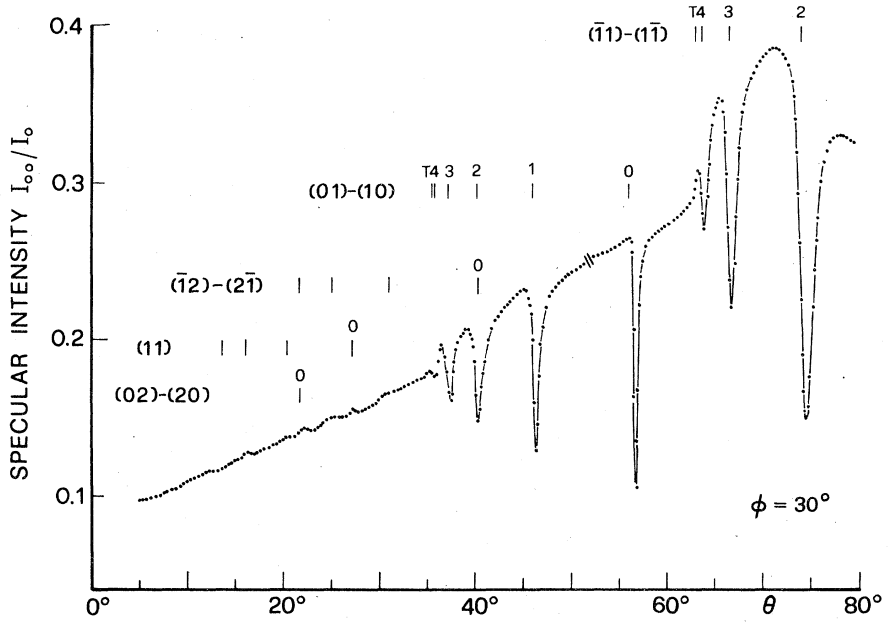

FIG. 2. Specular intensity at $\phi = 30°$ vs incident angle θ. For other comments see Fig. 1.

resonance positions. The associate wave vectors $\vec{G}$ should be the centers of the circles that constitute the loci of the resonances [see Eq. (1)]. A map of the position of the resonance minima is shown in Fig. 3 for the full azimuthal range $0° < \phi < 30°$; it is apparent that the points fall on arcs (except at the resonance crossings) whose centers are at the wave vectors with the indicated labels. The energy levels ϵ_m thus found for the three different $\vec{G}$ vectors are entirely consistent when the labels m are chosen as indicated in Fig. 3, with ϵ_0 representing the deepest level. The newly found energy levels enabled us, in turn, to estimate the positions of the resonances for *any* $\vec{G}$. The results are shown in Figs. 1 and 2. For completeness, aside from the five resonant levels the calculated threshold level for the continuum is also indicated.

The main hypothesis formulated concerned the identification of the resonances with the minima in the experimental pattern. Observe that the chosen $\vec{G}$ vectors belong to the first zone of the reciprocal lattice; for these vectors the choice made should be correct, since consistent values were obtained for the energy levels. However, such identification is not true for $\vec{G}$ vectors further away from the origin. In Fig. 1 the resonances that occur at small scattering angles and that are labeled (11)-(2$\bar{1}$) are seen as weak maxima (the ϵ_0 resonance of this set seems to interfere with the same level of the (02)-(2$\bar{2}$) set, giving rise to a peculiar double-peaked shape). From these observations and from those accumulated by Derry *et al.*[8] there is now conclusive evidence that the strongly coupled $\vec{G}$ vectors of the first zone give rise to resonance minima in the specular beam, while the other $\vec{G}$ vectors tend to produce weak maxima. Remarkably, the same basic results were obtained theoretically by several authors and reported in a string of papers[12,13,20] that appeared concurrently with the experiments. The case of (1$\bar{2}$)-($\bar{1}$2) resonances is discussed in greater detail in Sec. IV.

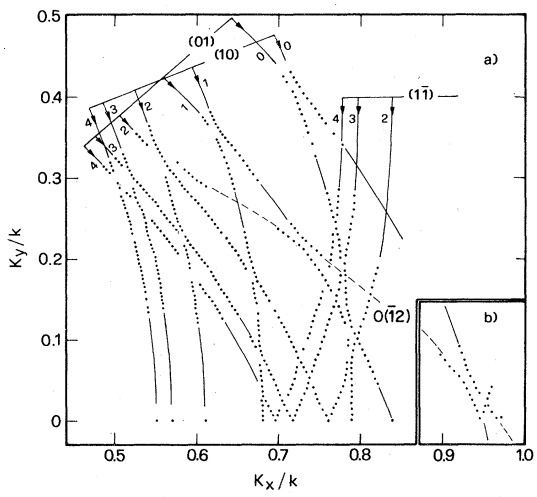

FIG. 3. Map of position of resonance minima in the reduced $\vec{K}$ plane. The incident wave vector was $k = 6.49$ Å^{-1} for all data shown except for those in inset (b), where $k = 6.82$ Å^{-1}. Crossings with or without splitting are recognized.

C. Determination of BSR levels

From the position of the BSR minima associated with different $\vec{G}$ vectors it was possible[5] to assign the following values (in units of meV) to the levels: $\epsilon_0 = -11.77 \pm 0.10$, $\epsilon_1 = -6.13 \pm 0.10$, $\epsilon_2 = -2.68 \pm 0.08$, and $\epsilon_3 = -0.83 \pm 0.06$ meV. A fifth minimum, corresponding to $+0.02 \pm 0.06$ meV, was identified as a threshold (T) resonance. However, to determine these absolute energy levels required greater precision in calibrating the zero in θ than our procedures allowed. With the aid of optical alignment techniques Derry *et al.*[8] were able to achieve in their spectrometer a very accurate determination of θ: in an experiment similar to ours, they identify the fifth minimum with a level $\epsilon_4 = 0.17 \pm 0.06$ meV. Using this value to adjust the zero in θ for every set of measurements, we have derived new values for the energy levels. The correction in θ amounted to 0.25 ± 0.10 degrees and the averaged new values are (in meV) $\epsilon_0 = -11.98 \pm 0.07$, $\epsilon_1 = -6.33 \pm 0.06$, $\epsilon_2 = -2.85 \pm 0.06$, $\epsilon_3 = -0.99 \pm 0.05$, $\epsilon_4 = -0.17 \pm 0.06$.[10]

Both an improvement in the standard deviations and an excellent overall agreement with the results obtained by Derry *et al.*[8] are thus obtained. The nature of the topmost level, as a resonance state rather than as a threshold, seems to be confirmed by its behavior at the crossing with other resonances. In at least one case the admixing of this resonance with the ϵ_0 state is observed. (See Fig. 6.)

D. Observation of resonance splittings

An overall view of the splittings at the intersection of resonances is presented in the reduced $\vec{K}$ plane in Fig. 3. Several crossings appear, mostly involving two resonances. For these, the resonances are split if the difference between the two $\vec{G}$ vectors is in turn a vector of the first zone; they are unsplit if $\vec{G}_1 - \vec{G}_2$ is a vector of higher order. It is evident from Eq. (2) that such observation can be translated into the assertion that, among the higher Fourier components of the surface potential, only V_{10} is non-negligible; this is in excellent agreement with the findings of the analysis of the diffracted intensities. Some of the crossings have a more complex structure. For example, a triple crossing appears near $K_x/k \sim 0.78$, $K_y/k \sim 0.10$ and a quadrupole crossing near $K_x/k \sim 0.56$, $K_y/k \sim 0.32$. In the latter case, a four-channel degeneracy is at work but, since two channels are associated with second-order $\vec{G}$ vectors, a negligible effect results, as can be seen [Fig. 2; resonance $0(\bar{1}2)$ and $2(01)$].

As can be seen in Fig. 3, some of the data points are missing at the crossing of symmetric levels [e.g., level ϵ_1 for the $\vec{G}$ vectors (01) and (10)]. This is due to the fact that one of the two minima vanishes at the crossing. This phenomenon, which was predicted by Chow[14] and studied in detail in a previous paper,[5] can be briefly described in the following way. At the crossing of two symmetric states the unperturbed wave functions of the individual states are essentially the same. Thus by choosing a proper combination of the wave functions, only one resonance condition is obtained at the crossing. The shift of the minimum from the resonance circle gives the sign of the potential. As can be observed in Fig. 2, for the $\phi = 30°$ azimuth the (10) and (01) admixed BSR's are unsplit but consistently shifted toward polar angles larger than those calculated in the free-atom approximation, thus showing that $V_{10}(z) < 0$. As will be shown below, the disappearance of one of the minima occurs not only at the crossing of symmetric states.

It seems worthwhile to examine in greater detail three interesting regions of crossing; to do this, the original experimental data, rather than the position of the minima, are shown in Figs. 4–6.

Figure 4 shows a region near the azimuth angle $\phi = 30°$. Admixing of (10) and (01) resonances is

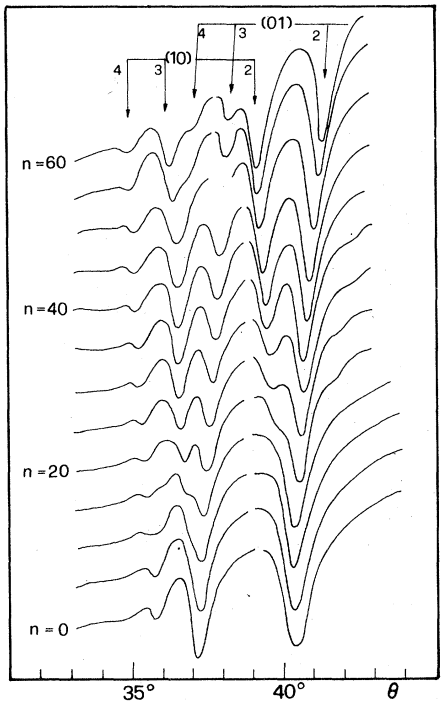

FIG. 4. Polar scans of specular intensity near azimuthal angle $\phi = 30°$; n is the number of turns of the azimuth driver (see Sec. II) as measured from the symmetry direction corresponding to $\phi = 30°$ ($n = 100$ corresponds to $\Delta\phi = -10.43°$).

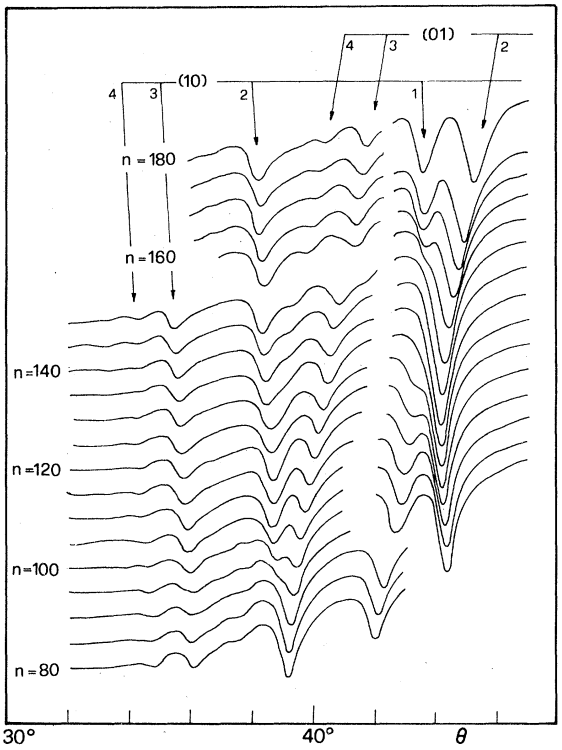

FIG. 5. Polar scans similar to those of Fig. 4, in an adjacent region of the $\vec{K}$ plane.

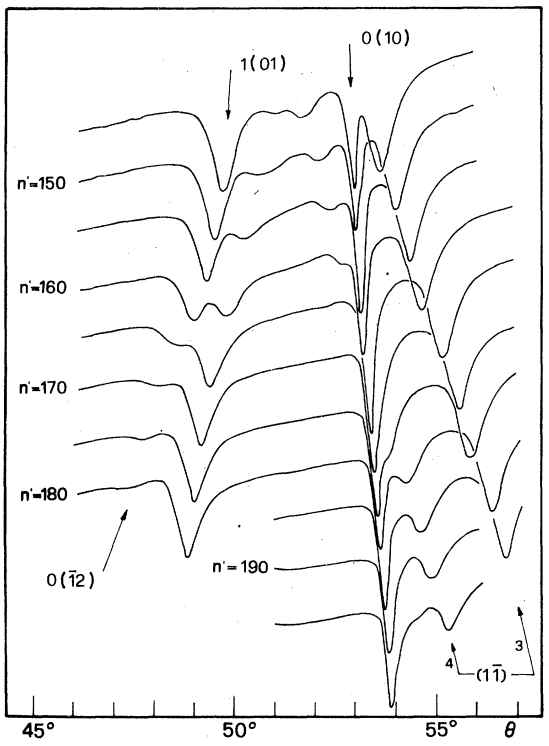

FIG. 6. Polar scans of specular intensity near azimuthal angle $\phi = 15°$; n' is measured from the symmetry direction corresponding to $\phi = 0°$ ($n' = 100$ corresponds to $\Delta\phi = 10.43°$).

taking place. Splitting is observed for both ϵ_2 and ϵ_3 levels, but it is not measurable for ϵ_4. The disappearance of one of the two minima can be clearly seen near $\phi = 30°$.

In Fig. 5 the admixtures of 2(10) with 3(01) and of 1(10) with 2(01) are shown; the "crossing" occurs at ϕ angles labeled by $n \sim 80$ and $n \sim 145$, respectively. In both cases the intensity of one of of the two resonances (that corresponding to the lower θ) goes to zero in the crossing region. The disappearance of a minimum is found to occur whenever two first-order resonances (i.e., resonances coupled by the smallest $\vec{G}$ vector to the specular beam) cross each other. Figure 5 also clearly displays the crossing of 2(10) with 4(01): here the splitting is unmeasurable.

Other examples of crossings are shown in Fig. 6. On the right-hand side the 0(10) resonance is seen to cross the $4(1\bar{1})$ resonance with a barely observable splitting. However, some admixture might take place, since the depth of the $4(1\bar{1})$ minimum does not seem to be symmetric across the intersection with the 0(01) resonance. In contrast, the crossing of $3(1\bar{1})$ with 0(10) shows a clear splitting and the intensities change in a fashion similar to that shown by the crossings in Fig. 5. On the left-hand side of Fig. 6 another interesting example of admixture can be seen. Here the faint $0(\bar{1}2)$ minimum crosses the first-order 1(01) resonance, borrowing intensity from the strong minimum in the admixing zone. This effect (of which another example was offered in a previous paper[5]) is present in graphite every time a first-order BSR crosses a second-order BSR and the two resonances are coupled by the smallest $\vec{G}$ vector.

No experimental evidence for splitting at the crossing of the BSR's coupled by (11) reciprocal-lattice vectors was found.

E. Evaluation of matrix elements

Let us assume that near the degeneracies the simple perturbation formula given by Eq. (2) is valid. By using this approximation the experimental data are easily treated and the matrix elements V_{10}^{mn} can be derived. The question remains whether the resonance loci coincide with the minima even near the crossing region.

Figures 7–9 are examples of how the treatment was made. The points show the positions of the experimental minima; the dashed lines represent the best-fit curves described by Eq. (2). Although some deviations are present, the fittings appear quite good.

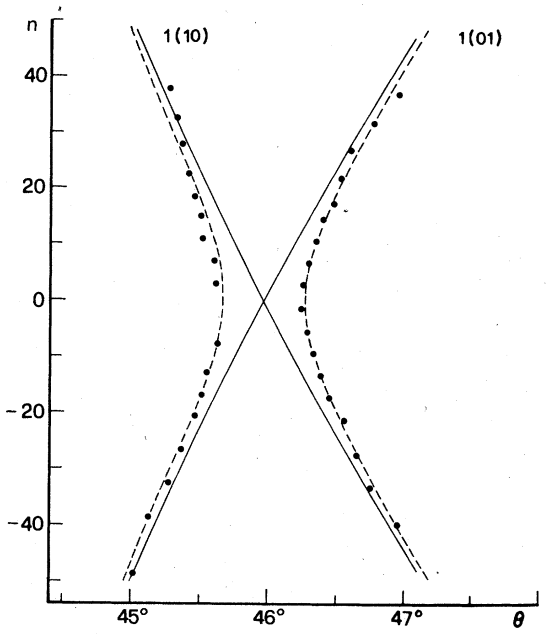

FIG. 7. Plot showing how the evaluation of the matrix element V_{10} was carried out. Points represent position of experimental minima. Full lines correspond to the free-atom approximation [Eq. (1)], while dashed lines represent curves described by Eq. (2) with $V_{10}^{11}=0.185$ meV.

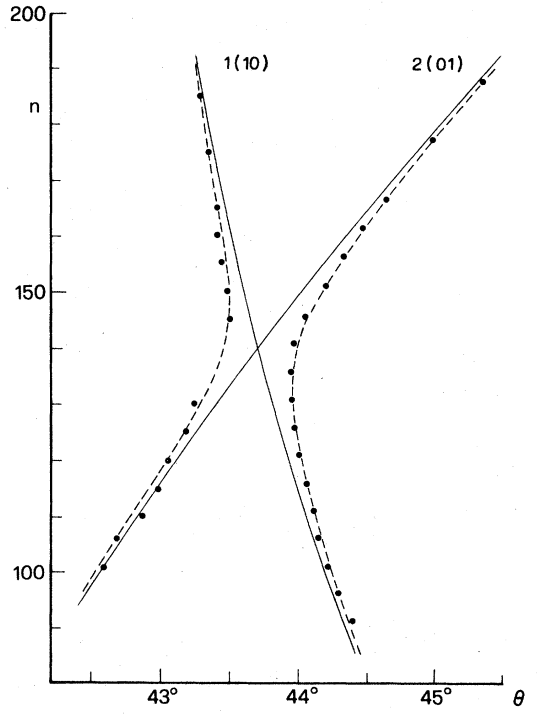

FIG. 8. Plot similar to that shown in Fig. 7. Dashed lines correspond to $V_{10}^{12}=0.160$ meV.

The matrix elements thus derived are reported in Table II together with their mean-square errors. One of them, V_{10}^{01} (briefly V^{01}), was obtained by carrying out three independent measurements: the crossing of $0(\bar{1}2)$ with 1(01) yielded 0.205 meV; that of 0(10) with 1(01) yielded 0.190 meV; and the last crossing, measured at $k=8.07$ Å^{-1}, yielded 0.195 meV. One can see that the spread in values is within the quoted mean-square error.

IV. LINE SHAPES OF RESONANCES

Since the number of BSR's is rather small and the number of crossings is limited, the He-graphite scattering at low incident energies is favorable to an analysis of line shapes and linewidths.

Figure 10 shows on an enlarged scale a typical isolated BSR minimum, 0(01) appearing in the specular beam at $\phi=30°$ and $\theta\sim56.5°$. As noted previously in connection with Fig. 2, this is an admixed resonance with only one minimum surviving. The line shape is asymmetric, showing a small shoulder followed by a steep decrease on the left and a more gradual increase on the right; the asymmetry is more pronounced here than in resonance minima observed in the scattering of He from LiF.[2] The observed width of the resonance is affected by instrumental effects, which are evaluated in the Appendix. With the known

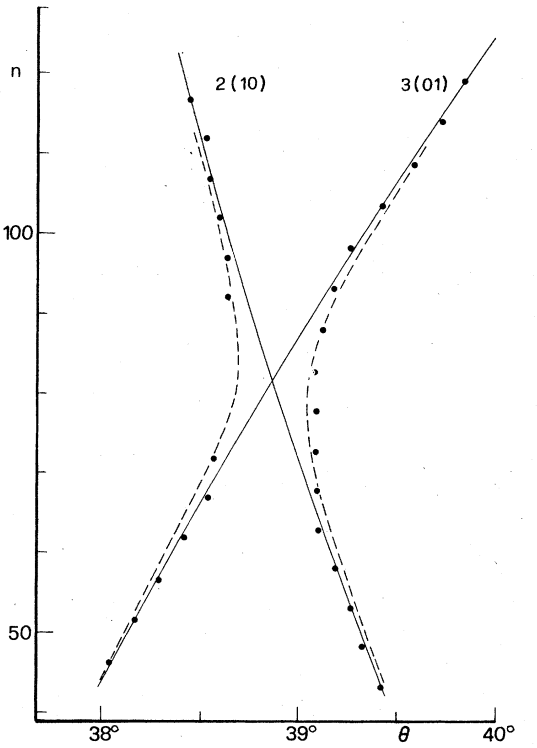

FIG. 9. Plot similar to that shown in Fig. 7. Dashed lines correspond to $V_{10}^{23}=0.110$ meV.

TABLE II. Experimental matrix elements $\langle \chi_m | V_{10} | \chi_n \rangle$ (meV).

$n \backslash m$	0	1	2	3
0	0.28 ± 0.01			
1	0.195 ± 0.015	0.185 ± 0.02		
2	0.125 ± 0.02	0.16 ± 0.015	0.12 ± 0.015	
3	0.09 ± 0.015	0.10 ± 0.01	0.11 ± 0.015	0.08 ± 0.025
4	0.03 ± 0.02	...	...	...

instrumental $\langle \Delta\theta_R^2 \rangle$ the intrinsic linewidth (FWHM) can be roughly obtained by

$$w_{\mathrm{FWHM}} = (\langle \Delta\theta^2_{\mathrm{expt}} \rangle - \langle \Delta\theta_R^2 \rangle)^{1/2} . \quad (4)$$

This simple formula gives only an approximation of the true FWHM, since it assumes that the line shape of the resonances has a Gaussian form, whereas in reality it is (at best) a Lorentzian. For the resonance shown in Fig. 10 the experimental width is $\Delta\theta_{\mathrm{expt}} \simeq 0.35°$ and $\langle \Delta\theta_R^2 \rangle^{1/2} \simeq 0.19°$, so that $w_{\mathrm{FWHM}} \simeq 0.29°$, corresponding to an energy width $\Gamma_0 = 0.14$ meV.

Using the same procedure, the linewidths of all resonance minima appearing in Figs. 1 and 2 were evaluated. The results are given in Table III, where the subscript to Γ indicates the vibrational level. The widths appear to depend essentially on the level index, and very little on the $\vec{G}$ vector

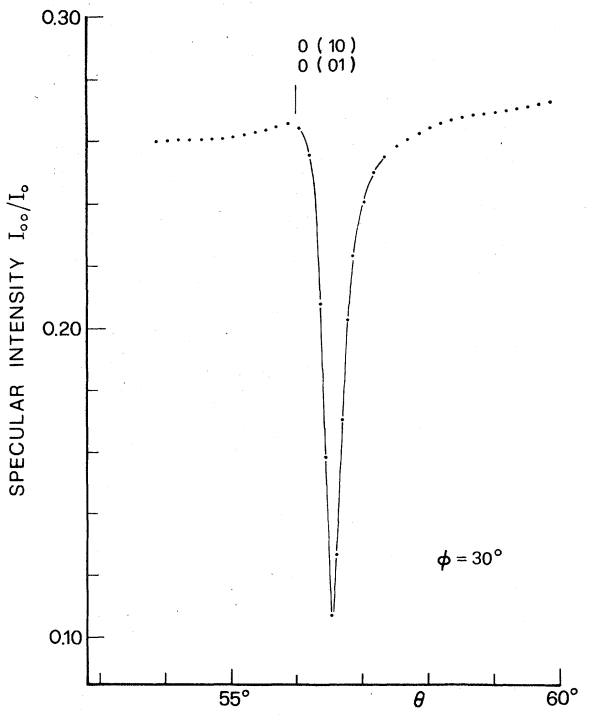

FIG. 10. Line shape of 0(10)-0(01) admixed resonance at $\phi = 30°$.

characterizing the resonance. The anomalous Γ given for the 1(10) resonance is caused by estimation difficulties due to the proximity of other resonances (see Fig. 12).

All resonance minima in the specular beam exhibit the peculiar asymmetric line shape described in the comments to Fig. 10. Figures 11 and 12 show on an enlarged scale some of the features of Fig. 1 ($\phi = 0$). The isolated minima possess systematically a small shoulder at the lower side of θ and a gentler slope at large θ. The 0(10) resonance is, however, an exception to this trend. For this resonance the line shape appears to be more symmetrical around the minimum, with the shoulder now to the right. The only feature which distinguishes this resonance from the others belonging to the same (10) family is that at its incident angle the (01) and $(1\bar{1})$ channels are closed; as a consequence, the 0(10) resonance is coupled only to the specular diffraction peak. This fact, as was pointed out by Wolfe and Weare,[12] may affect the line shape of a resonance.

Another resonance family is also present in the region shown in Fig. 12, namely, that associated to $(1\bar{2})$ and $(\bar{1}2)$ unsplit closed channels. These resonances appear as weak structures (see ϵ_3 and ϵ_4 in the region around 40°) and their shape is not clear. In contrast, the ϵ_0 resonance of this family, presented in Fig. 1, closely resembles a minimum. Such complex behavior may be due to the interaction of pairs of resonances [the $(1\bar{2})$ and the $(1\bar{1})$ families; the $(\bar{1}2)$ and the (01) families] that cross each other at azimuthal angles close to $\phi = 0°$. In an attempt to clarify these features, we measured (Fig. 13) the diffraction probability of the $(\bar{1}0)$ peak. Although the general trend is simi-

TABLE III. Linewidths (FWHM) of resonance minima (meV).

ϕ	$\vec{G}$ vector	Γ_0	Γ_1	Γ_2	Γ_3	Γ_4
0°	(10)	0.14	(0.42)	0.38	0.22	0.16
0°	(01)-$(1\bar{1})$	0.16	0.34	0.32	0.23	...
30°	(10)-(01)	0.14	0.28	0.35	0.21	0.15
30°	$(\bar{1}1)$-$(1\bar{1})$	...	...	0.32	0.21	0.12

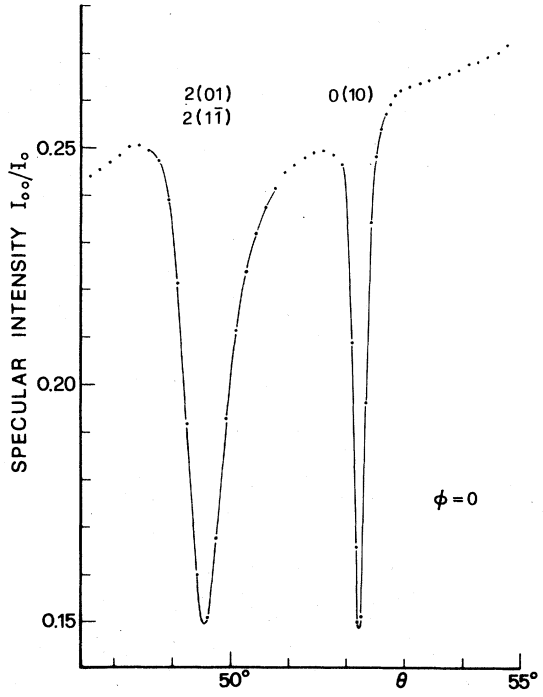

FIG. 11. Line shapes of two resonances appearing at $\phi = 0°$.

lar to that of the (00) peak, a few differences between the shapes of the resonances are noticeable. The minima are more symmetric; those associated with (01) and (1$\bar{1}$) $\vec{G}$ vectors appear to be deeper and the asymmetry in their shape has the reverse trend of the corresponding minima shown in Fig. 1. In addition, the ($\bar{1}$2)-(1$\bar{2}$) resonance family displays more pronounced structures having a peculiar maximum-minimum shape, as is clear for ϵ_3 at $\theta \sim 41°$. Once again, a strong admixture is noticeable owing to the near-crossing condition of 0(01) and 0($\bar{1}$2) resonances (and the equivalent ones, by symmetry). The two minima have almost the same depth and their line shapes are different from the corresponding ones in the (00) beam.

The BSR features described in this section should be of great value for any detailed comparison of the experiment with theoretical models.

V. DISCUSSION

The experimental quantities presented here will now be used to test the analytical forms of the gas-surface potential that have been proposed in the literature. We will begin with the bound-state resonance levels ϵ_m. As is observed in Ref. 4, neither a Morse potential nor a 3-9 potential can accurately represent the experimental vibrational spectrum of He-graphite. In order to discuss the data and to give a more accurate description of $V_0(z)$, the three-parameter model potential

$$V(z) = D[(1+\lambda z/n)^{-2n} - 2(1+\lambda z/n)^{-n}] \qquad (5)$$

will be used. This potential, first suggested by Tommasini and co-workers,[15] adequately interprets the vibrational spectrum of H and D selectively absorbed on graphite. The potential parameters are determined by a numerical best fit of the experimental ϵ_m's to the eigenvalues of Eq. (5). Using this procedure, the well depth D is found to be 15.70 meV, while the inverse-length parameter

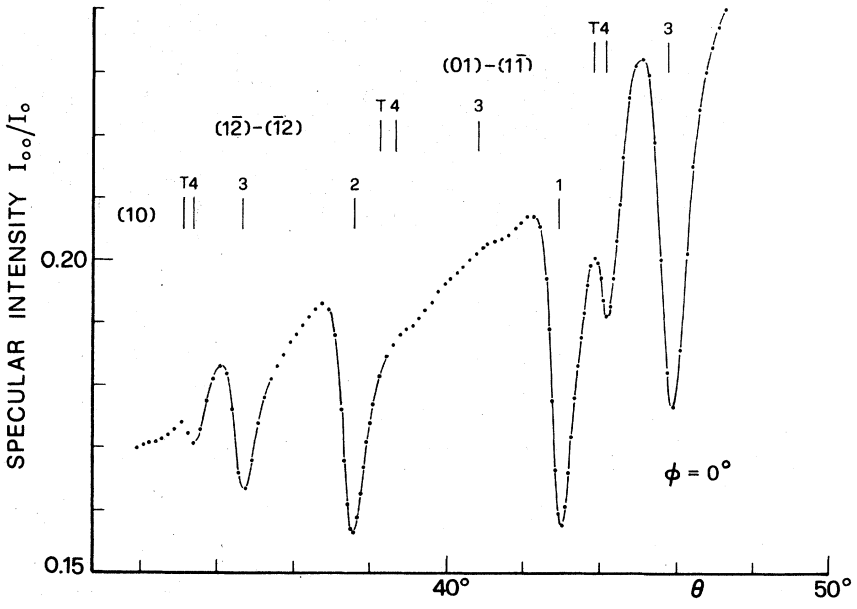

FIG. 12. Enlarged portion of Fig. 1 showing line shapes of selected resonances.

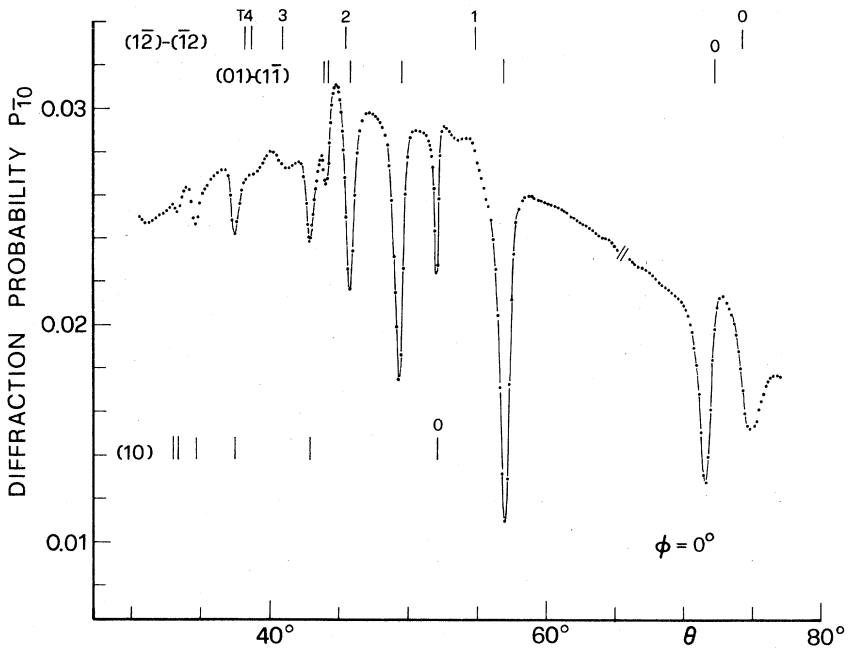

FIG. 13. $(\bar{1}0)$ diffraction probability at $\phi = 0°$ vs incident angle θ. Compare with Fig. 1.

λ is 1.413 Å^{-1} and the exponent n is 5.3. It is notable that the exponent n found in Ref. 15 for the system H-graphite is 5.1; this means that the two exponents may be considered to be equal within experimental errors. In Table IV a comparison is made between the experimental levels and the theoretical eigenvalues of Eq. (5) when the parameters given above are used. In the same table are given the eigenvalues of the shifted Morse potential,[16]

$$V(z) = D(x^2 - 2x - \Delta), \tag{6}$$

with $x = \exp(-\alpha z)$ and best-fit parameters $D = 14.59$ meV, $\alpha = 1.347$ Å^{-1}, and $\Delta = 0.058$.

The Morse potential, which allows simpler analytical solutions, seems to be a slightly worse representation of the true surface-averaged potential $V_0(z)$ than the potential given by Eq. (5).

In order to derive information on the first Fourier component of the overall gas-surface potential, a parameterization of the form

$$V_{10} = -\beta D(1 + \lambda z/n)^{-\alpha n} \tag{7}$$

was adopted. The matrix elements of Eq. (7) were calculated by means of Eq. (3), where χ_m and χ_n were numerically evaluated from the potential in Eq. (5). It was found that the choice $\alpha = 3$ gives a much better fit to the experimental data than the more conventional $\alpha = 2$.[17] The results are shown in Table IV. The second column of Table IV contains the matrix elements calculated by using $\alpha = 2$ and $\beta = 0.022$, and the third with $\alpha = 3$ and $\beta = 0.019$. An α value of 3 seems to give to $V_{10}(z)$ the steepness which is required in order to explain the large experimental values of V^{03}, V^{13}, V^{23}, and V^{33}.

The matrix elements calculated with the Morse potential and with the related Fourier component $V_{10} = -\beta D x^2$ are shown for comparison in the first column of Table IV. The best-fit value for β is

TABLE IV. Energy levels and matrix elements of V_{10} calculated with shifted Morse (SM) and Tommasini potentials (meV).

Energy level	SM	Tommasini		Expt.
ϵ_0	11.95	11.96		11.98
ϵ_1	6.41	6.36		6.33
ϵ_2	2.77	2.85		2.85
ϵ_3	1.02	0.95		0.99
ϵ_4	···	0.16		0.17
Matrix element	SM	Tommasini $\alpha = 2$	Tommasini $\alpha = 3$	Expt.
V^{00}	0.279	0.290	0.274	0.280
V^{11}	0.197	0.188	0.203	0.185
V^{22}	0.116	0.109	0.127	0.120
V^{33}	0.036	0.052	0.063	0.080
V^{01}	0.156	0.156	0.195	0.195
V^{02}	0.090	0.093	0.133	0.125
V^{03}	0.043	0.057	0.086	0.090
V^{04}	···	0.032	0.050	0.030
V^{12}	0.132	0.123	0.153	0.160
V^{13}	0.067	0.077	0.103	0.100
V^{23}	0.063	0.072	0.088	0.110

0.020. One can see that such repulsive potential does not fit the experimental data very well. This is hardly surprising, since its rise is significantly slower than that of the potential in Eq. (7).

While the experimental values of ϵ_m and V^{mn} impose strong constraints on the shapes of $V_0(z)$ and $V_{10}(z)$ in the region of the well, they give little information on these shapes in the region $V_0 > 0$. The only information about this region comes from the intensity distribution among diffraction peaks. It is now understood that this intensity distribution depends not separately on $V_0(z)$ and $V_{10}(z)$ but essentially on the corrugation amplitude, which is strictly related to the variation of the classical turning point within the surface unit cell. As reported in Sec. III, no variation of the corrugation was detected experimentally over the incident energy range 20–65 meV. Therefore the repulsive potential curves corresponding to different points of the unit cell appear to run up quite parallel to each other. This condition is fulfilled neither by the Morse potential nor by the potential described in Eqs. (5) and (7). We can add that any $V_{10}(z)$ that is merely a modulation of the repulsive term of the model potential is also unacceptable. In other words, a potential expressed by $V_0(z) = V_R(z) + V_A(z)$ and by $V_{10}(z) = \beta V_R(z)$, frequently used in past studies, does not give, in general, a constant corrugation within the relevant energy range. This occurs only if the potential takes an infinite slope over that range.

A model potential that proved to be more useful is explaining the intensity distribution among diffraction peaks is the hard corrugated surface with a well.[11] Garcia[18] recently used a variation of this model to carry out extensive calculations of diffraction intensities and resonances for the He-graphite system. In order to approach the true potential in the region of the well, Garcia used an attractive well with a flat botton and with a $1/z^3$ dependence at large distances. He was able to reproduce with remarkable accuracy the experimental intensities and the bound-state anomalies; his values for ϵ_m and V^{mn} are only in qualitative agreement with the experimental results. The asymptotic behavior of $V_0(z)$ for $z \to \infty$ is expected to follow a $1/z^3$ law. Although the potential in Eq. (5) has the "wrong" form, it still accurately represents the vibrational levels near dissociation for both He and H. Thus is appears that the $1/z^3$ dependence becomes effective at quite a distance from the well minimum.

In conclusion, none of the simple analytical expressions hitherto proposed for the He-graphite potential seems consistent with the full ensemble of the experimental data. More direct calculations of the potential are now appearing in the literature. Among these is the semiempirical evaluation made by Steele.[19] Steele's potential, constructed from a sum of pairwise atom-atom potentials, was used by Chow[20] to perform close-coupling calculations on band-structure effects upon scattering. Chow's results are in qualitative agreement with our experimental findings. On the basis of our first results,[4] Steele's potential was improved by Carlos and Cole.[21] We are now informed by these authors that a sum of pairwise interactions which takes into account the anisotropy of the attractive term gives a very good fit to the available experimental data.[22] The proposed potential very much resembles that described by Eqs, (5) and (7), at least in the region of the well.

Finally, we would like to make a few comments about the BSR line shapes. The occurrence of minima or maxima is correctly predicted by the rules given by Wolfe and Weare[12] and by Celli, Garcia, and Hutchinson[13]; in both studies only elastic scattering was considered. The latter authors pointed out that important information is contained in the line shape of a given resonance and predicted that for He-graphite the isolated minima would not display a Lorentzian shape; rather, they would be asymmetric owing to the hexagonal surface symmetry. This was confirmed by the experiment. Moreover, the same authors gave the following expression for the linewidth (FWHM):

$$\Gamma = 2\left(\frac{d\delta}{d\epsilon}\right)^{-1}(1 - |S|), \tag{8}$$

where $d\delta/d\epsilon$ is the density of bound states and $(1 - |S|)$ gives the total scattering probability out of the resonant state. The last factor increases when going from ϵ_0 to ϵ_4, whereas $(d\delta/d\epsilon)^{-1}$ goes rapidly to zero as the continuum threshold is approached. The experimental trend of linewidths shown in Table III is well described by Eq. (8). Yet the agreement is not quantitative: in particular, the measured width of resonances is larger than expected near the dissociation limit.

More accurate measurements of line shapes and linewidths may provide the critical test for verifying whether the elastic theory[23] is sufficient to describe all observed features of resonance structures.

ACKNOWLEDGMENTS

We would like to acknowledge informative and stimulating discussions with M. Cole, N. Garcia, and F. Tommasini, and a very profitable correspondence with V. Celli and W. Carlos. To all of them we are grateful for having sent us results in advance of publication. This work was suppor-

ted in part by NATO Research Grant No. 1407. The work of one of us (G.P.F.) was supported by the U. S. Department of Energy.

APPENDIX: EXPERIMENTAL RESOLUTION FUNCTION

For the purpose of this experiment our measurements were confined to in-plane scattering. The angular divergence of the beam in this plane is denoted by $\Delta\theta_i$ and the divergence off the plane is $\Delta\xi$, where ξ is the azimuthal angle with the scattering plane; the spread of wave vectors is Δk_i. Let us assume that these quantities are independent and that the intensity profile of the incident beam is given by

$$I(\Delta\theta_i, \Delta\xi, \Delta k_i) = I_0 \exp\{-[a^2(\Delta\theta_i)^2 + b^2(\Delta k_i)^2 + c^2(\Delta\xi)^2]\}, \quad \text{(A1)}$$

where the experimental widths are

$$\langle \Delta\theta_i^2 \rangle^{1/2} = 0.15^\circ,$$

$$\langle \Delta\xi^2 \rangle^{1/2} = 0.30^\circ,$$

and

$$\langle \Delta k_i^2 \rangle^{1/2} = 0.02 k_i .$$

Now let us calculate the linewidth $\langle \Delta\theta_R^2 \rangle^{1/2}$ of a resonance due to the resolution of the beam.

In the described coordinate system, the resonance condition in Eq. (1) may be written

$$(k_i \sin\theta_i + G\cos\xi)^2 + G^2 \sin^2\xi = k_i^2 - 2m\epsilon_j/\hbar^2 . \quad \text{(A2)}$$

When the center of the beam is at an angle $\theta = \theta_i + \theta_R$ with the crystal, a portion of the beam still satisfies the resonance condition. The required mis-set of k_i is, in the first approximation,

$$\Delta k_i = A(\Delta\theta_i - \Delta\theta_R) + B\Delta\xi , \quad \text{(A3)}$$

with

$$A = \frac{k_i \cos\theta_i (k_i \sin\theta_i + G\cos\xi)}{k_i \cos^2\theta_i - G\cos\xi \sin\theta_i} \quad \text{(A4)}$$

and

$$B = \frac{k_i G \sin\theta_i \sin\xi}{G\cos\xi \sin\theta_i - k_i \cos^2\theta_i} . \quad \text{(A5)}$$

The portion of the beam that satisfies the resonance condition is

$$I_{\rm tot}(\Delta\theta_R) = I_0 \int_{-\infty}^{\infty}\int_{-\infty}^{\infty} \exp(-\{a^2(\Delta\xi_i)^2 + b^2[A(\Delta\theta_i - \Delta\theta_R) + B\Delta\xi]^2 + c^2(\Delta\xi)^2\}) d\Delta\theta_i\, d\Delta\xi . \quad \text{(A6)}$$

The argument of exp in the integrand represents the hellipsoid of resolution. Equation (A6) can be written in a more convenient form:

$$I_{\rm tot}(\Delta\theta_R) = I_0 \exp[-s^2(\Delta\theta_R)^2] \int_{-\infty}^{\infty}\int_{-\infty}^{\infty} \exp\{-[m^2(\Delta\theta_i - n\Delta\theta_R)^2 + p^2(\Delta\theta_i - n\theta_R)(\Delta\xi - q\Delta\theta_R) + r^2(\Delta\xi - q\Delta\theta_R)^2]\} d\Delta\theta_i\, d\Delta\xi , \quad \text{(A7)}$$

where all the coefficients in the integrand are independent of $\Delta\theta_R$. Hence the integral is the same for all angles of incidence around a given resonance. The factor preceding the integral defines the width of the resonance due to resolution function. The explicit dependence of $s^2 \equiv \langle \Delta\theta_R^2 \rangle^{-1}$ on the coefficients a, b, c, A, and B previously defined is

$$s^2 = a^2 b^2 c^2 \frac{(a^2B^2 + A^2c^2)(a^2 + b^2A^2) + 4A^4B^2b^2}{[a^2(b^2B^2 + c^2) + (b^2A^2c^2)]^2} . \quad \text{(A8)}$$

Note that a partial focalization of the beam occurs when $k_i \cos^2\theta_i = G\cos\xi \sin\theta_i$ [see Eqs. (A4) and (A5)].

[1] See, for example, W. A. Steele, *The Interaction of Gases with Solid Surfaces* (Pergamon, Oxford, 1974).
[2] D. R. Frankl, D. Wesner, S. V. Krishnaswamy, G. Derry, and T. O'Gorman, Phys. Rev. Lett. 41, 60 (1978).
[3] H. Chow and E. D. Thompson, Surf. Sci. 59, 225 (1976).
[4] G. Boato, P. Cantini, and R. Tatarek, Phys. Rev. Lett. 40, 887 (1978).
[5] G. Boato, P. Cantini, R. Tatarek, and G. P. Felcher, Surf. Sci. 80, 518 (1979).
[6] R. E. Elgin and D. L. Goodstein, Phys. Rev. A 9, 2657 (1974).
[7] E. J. Derderian and W. A. Steele, J. Chem. Phys. 66, 2831 (1977).
[8] G. Derry, D. Wesner, W. Carlos, and D. R. Frankl (unpublished).
[9] G. Boato, P. Cantini, and L. Mattera, Surf. Sci. 55, 141 (1976).
[10] This is the value obtained by Derry *et al.* (Ref. 8).
[11] U. Garibaldi, A. C. Levi, R. Spadacini, and G. E. Tommei, Surf. Sci. 48, 649 (1975).
[12] K. L. Wolfe and J. H. Weare, Phys. Rev. Lett. 41, 1663 (1978).
[13] V. Celli, N. Garcia, and J. Hutchison (unpublished).
[14] H. Chow, Surf. Sci. 66, 22 (1977).
[15] E. Ghio, L. Mattera, C. Salvo, F. Tommasini, and

U. Valbusa (unpublished).
[16]See C. Schwartz, M. V. Cole, and J. Pliva, Surf. Sci. 75, 1 (1978).
[17]Letting $\alpha = 2$ simply amounts to a modulation of the repulsive term of the potential in Eq. (5).
[18]N. Garcia, F. O. Goodman, V. Celli, and N. R. Hill, Phys. Rev. B 19, 1808 (1979).
[19]W. A. Steele, Surf. Sci. 36, 317 (1973).
[20]H. Chow, Surf. Sci. 79, 157 (1979).
[21]W. E. Carlos and M. W. Cole, Surf. Sci. 77, L173 (1978); N. Garcia, W. E. Carlos, and M. W. Cole (unpublished).
[22]W. E. Carlos and M. W. Cole, Phys. Rev. Lett. 43, 697 (1979).
[23]Calculations of line shapes by making use of an optical potential were recently carried out by Y. Hamauzu [J. Phys. Soc. Jpn. 42, 961 (1977)], H. Chow and E. D. Thompson [Surf. Sci. 82, 1 (1979)], and H. Chow (Ref. 20).